Letter

Inhomogeneous Biexciton Binding in Perovskite Semiconductor Nanocrystals Measured with Two-Dimensional Spectroscopy

Xinyu Huang,[§] Lan Chen,[§] Chunfeng Zhang,* Zhengyuan Qin, Buyang Yu, Xiaoyong Wang, and Min Xiao*

ACCESS | 📊 Metrics & More | 📰 Article Recommendations | 🆂🆃 Supporting Information

ABSTRACT: Perovskite semiconductor nanocrystals have emerged as an excellent family of materials for optoelectronic applications, where biexciton interaction is essential for optical gain generation and quantum light emission. However, the strength of biexciton interaction remains highly controversial due to the entangled spectral features of the exciton- and biexciton-related transitions in conventional measurement approaches. Here, we tackle the limitation by using polarization-dependent two-dimensional electronic spectroscopy and quantify the excitation energy-dependent biexciton binding energy at cryogenic temperatures. The biexciton binding energy increases with excitation energy, which can be modeled as a near inverse-square size dependence in the effective mass approximation considering the quantum confinement effect. The spectral line width for the exciton−biexciton transition is much broader than that for the ground state to exciton transition, suggesting weakly correlated broadening between these transitions. These inhomogeneity effects should be carefully considered for the future demonstration of optoelectronic applications relying on coherent exciton−biexciton interactions.
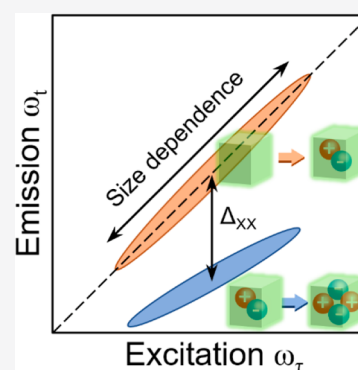
Perovskite semiconductors have recently emerged as excellent candidates for next-generation optoelectronic devices. Quantifying the interactions between electron−hole pairs has been pivotal in elucidating the exact physics underlying the high performances of light/electricity conversion devices.[1−4] Benefiting from the quantum confinement effects, perovskite semiconductor nanocrystals have been used to further promote the emission of light from excitonic states,[5−7] showing promising potentials for applications such as lasers,[8,9] light-emitting diodes (LEDs),[7,10] polariton condensation devices,[11,12] and quantum light sources.[13−16] In the devices, the interactions between multiple excitons generated in single nanocrystals are fundamentally important for device performance.[14,17−20] For instance, the formation of biexcitons can effectively generate an optical gain in perovskite semiconductor nanocrystals.[21,22] The brightness of LEDs under high-density excitations is highly sensitive to biexciton Auger recombination. Biexciton recombination complicates the fine structures of the emission of light from single nanocrystals, which has the potential to demonstrate entangled photon pairs via biexciton−exciton cascade emission by manipulating the coherent exciton−biexciton interactions.[15,16,23−26]

The strength of the interaction between two excitons in single nanocrystals can be quantified in terms of biexciton binding energy (Δ_{XX}), i.e., the energy shift for a biexciton ($|XX\rangle$) to exciton ($|X\rangle$) transition relative to the exciton ($|X\rangle$) to ground state ($|G\rangle$) transition.[27] In spite of the importance of biexciton interaction in understanding the optical properties that are technically significant, the interaction strength of

biexcitons in perovskite semiconductor nanocrystals remains elusive.[17,19,28−30] The biexciton binding energies in perovskite semiconductor nanocrystals have been intensively characterized by utilizing a broad range of methods, including temporally and spectrally resolved PL measurements[17,30] or transient absorption (TA) spectroscopy.[14,29,31,32] However, whether the biexciton interaction in $CsPbBr_3$ nanocrystals is repulsive[28] or attractive[19] is unknown. The reported values of biexciton binding energy in $CsPbBr_3$ nanocrystals have been diversely scattered over one order of magnitude in the range of 5−100 meV.[9,14,17,28−31] In addition to differences in prepared samples, these conflicting results may be caused by the sample modifications induced by air exposures and/or high-flux excitations during the conventional measurement approaches.[30] Moreover, the nanocrystal samples were prepared with inherent size diversity with a typical inhomogeneous line width for excitonic transitions at the level of 100 meV. The effect of inhomogeneity on the biexciton binding energy has been averaged out at the ensemble level. In principle, such an inhomogeneous effect can be evaluated by employing single-dot measurements. Nonetheless, the dot-to-dot variation of the

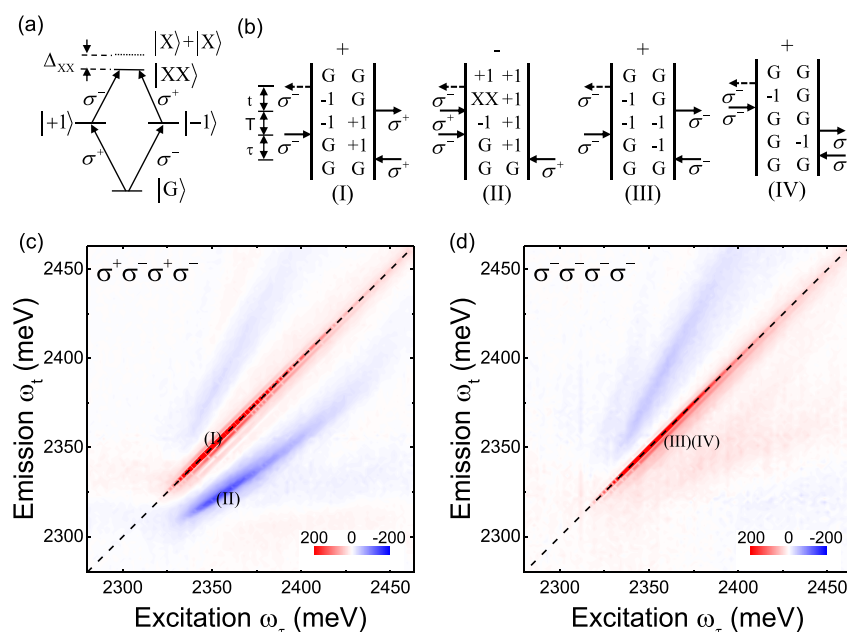© 2020 American Chemical Society

10173
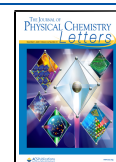
Figure 1. Polarization-dependent 2D spectra for CsPbBr$_3$ nanocrystals. (a) Energy level scheme indicating the excitation of the biexciton state through two cross-circularly polarized pulses with the ground state ($|G\rangle$), the one-exciton state ($|\pm1\rangle$), and the biexciton state ($|XX\rangle$). The one-exciton states are labeled by the total angular momentum $J = +1$ and -1. The left- and right-circularly polarized excitations are denoted as σ^+ and σ^-, respectively. (b) Double-sided Feynman diagrams representing the quantum pathways for the cross-circularly polarized (I and II) and co-circularly polarized (III and IV) configurations. The plus or minus sign above the corresponding diagram indicates the signal phase of the corresponding diagram. Real parts of rephasing 2D spectra of CsPbBr$_3$ nanocrystals at 10 K with the (c) cross-circular and (d) co-circular excitations. The population delay time is 100 fs.

specific emission energy and the relative broad line width make it extremely challenging to fully survey the size-dependent Δ_{XX}.

In this work, we overcome these limitations by using two-dimensional electronic spectroscopy (2DES) and succeed in quantifying the inhomogeneous biexciton binding energy in CsPbBr$_3$ nanocrystals at cryogenic temperatures. 2DES probes the third-order nonlinear optical response induced by three sequenced optical pulses with precisely controlled phases, establishing the correlation between the excited and probed states with high energy and time resolutions.[33−37] The transitions between exciton and biexciton states can be explicitly isolated with weak optical excitation under the proper configuration of pulse polarizations.[38,39] Of particular importance is the fact that the disentanglement capability of the inhomogeneous line width makes 2DES ideal for investigating the size-dependent biexciton interactions with ensemble samples.[40,41] The biexciton interaction in CsPbBr$_3$ nanocrystals is characterized as being attractive with a binding energy in the range of 25−40 meV having a near linear correlation to the exciton energy (E_X), which can be explained as the size dependence by theoretical consideration under the effective mass approximation (EMA). The value of Δ_{XX} is found to show an inverse-square dependence on the nanocrystal size, which is nearly independent of temperature (< 100 K), suggesting that quantum confinement is primarily responsible for the enhanced biexciton binding energy in nanocrystals with respect to that in bulk samples.

The samples of CsPbBr$_3$ nanocrystals were synthesized following the approach described in the literature.[7,22] To study the size-dependent effect, we selected an ensemble of samples with a relatively broad size distribution with an average size of ∼9 nm (Figure S1). Because the effective Bohr diameter is ∼7 nm for CsPbBr$_3$,[7] the nanocrystals can be considered to be in

the weak/intermediate confinement regime that is used in most optoelectronic devices.

2DES experiments were performed using the pulses generated from a non-collinear optical parameter amplifier (see the Supporting Information for details) with spectra covering the low-lying excitonic transitions centered at ∼2.36 eV (Figure S2).[42] The pulse duration was ∼14 fs as diagnosed by a fringe-resolved autocorrelator. We conducted 2DES using a partially collinear configuration with a pump-probe geometry as described in detail in the Supporting Information (Figure S3) and the previous method paper.[42] Two phase-stabilized replicas with time interval τ were employed as the pump pulses. The probe pulse was set with population time delay T equal to the second pump pulse. The field of the nonlinear optical response in transmission geometry was captured using the probe pulse as the local oscillator that was then analyzed with a fast spectrometer to generate the spectra in emission domain ω_t (Supporting Information). Herein, we show the amplitude of the 2D signal (A_{2D}) of the real part of the rephasing pulse sequence[43] in the domains of excitation energy (ω_τ) and emission energy (ω_t) at different population time delays (T).

As shown schematically in Figure 1a, left- and right-circularly polarized (σ^+ and σ^-, respectively) excitations populate the excitonic states with specific angular momentums ($J = 1$ or −1). The low-lying biexciton state can be directly populated by two pulses configured with crossly circular polarizations. We use the cross-circularly polarized ($\sigma^+\sigma^-\sigma^+\sigma^-$) and co-circularly polarized ($\sigma^-\sigma^-\sigma^-\sigma^-$) configurations in 2DES experiments to distinguish the signals related to the biexciton states (Figure 1b). The Feynman diagrams that contribute to the rephasing four-wave mixing (FWM) signal are shown in Figure 1b. With the cross-circularly polarized pulse sequence, the FWM signal
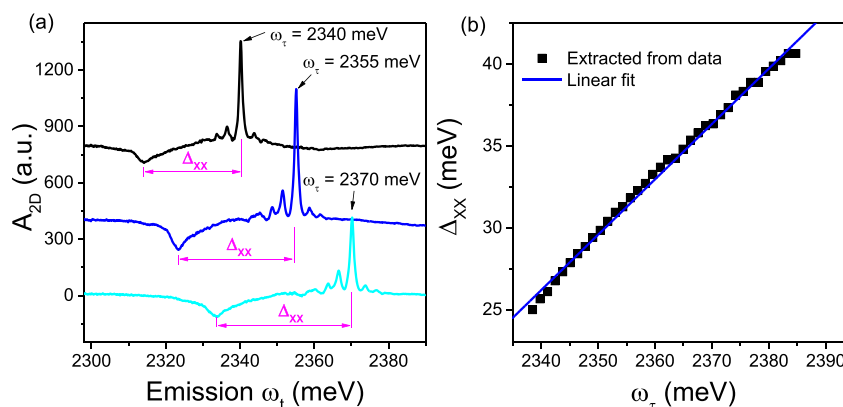
Figure 2. Excitation energy-dependent biexciton binding energy. (a) Emission spectra extracted from cross-circularly polarized 2D spectra with excitation energies (ω_τ) of 2340, 2355, and 2370 meV. The amplitude (A_{2D}) of the real part of the 2D signal in the rephasing pulse consequence is shown as a function of excitation energy. Biexciton binding energy Δ_{XX} can be evaluated by the difference between energies resonant to exciton and biexciton features. (b) Derived biexciton energy plotted as a function of excitation energy. The solid line shows a linear fit.

contains a positive part (I in Figure 1b) and a negative part (II in Figure 1b). The negative part involves the transition between the $|X\rangle$ and $|XX\rangle$ states. With the co-circularly polarized pulse sequence, the FWM signal contains two positive parts (III and IV in Figure 1b), which involve the transitions between the ground state and single exciton state only. The different pathways involved in the 2DES signal recorded with different polarization configurations allow the isolation of the signal related to the $|X\rangle \rightarrow |XX\rangle$ transition with a weak excitation level of ~1 $\mu J/cm^2$. The average number of excitons per nanocrystal is estimated by multiplying the absorption cross section and the incident photon flux, which is <0.1, avoiding the high-flux excitation required by conventional measurement approaches.

The 2D spectra of $CsPbBr_3$ nanocrystals at 10 K with the cross-circularly and co-circularly polarized excitations are shown in panels c and d of Figure 1, respectively. The population time (T), i.e., the time delay between the second and third laser pulses, was set at 100 fs. The cross-circularly and co-circularly polarized 2DES spectra both show positive signals at the diagonal position. The diagonal signals in panels c and d of Figure 1 correspond to the Feynman diagram (I), (III) and (IV), respectively, where the excitation energy (ω_τ) and the emission energy (ω_t) are resonant to the excitonic transition (E_x). The $|X\rangle \rightarrow |XX\rangle$ transition is manifested as the difference between the cross-circularly and co-circularly polarized spectra, i.e., the negative signal below the diagonal (II, Figure 1c). In $CsPbBr_3$ nanocrystals with no static spin order, the cross-polarization-selective feature (II) is a characteristic signature of doubly excited states. With a near-resonant excitation, the bound biexciton is such a state of double excitation as well established in previous studies of biexcitonic interaction in semiconductor nanostructures.[39,44,45] The negative signal is observed with the downshift of the emission energy to the excitation energy, which is similar to the biexciton feature uncovered in TA spectroscopic studies.[14,31,32,46] Moreover, power-dependent PL measurements suggest a similar energy red-shift of biexciton emission to excitonic emission (Figure S4). These corroborated results strongly support the assumption that the feature (II) is induced by the transition from exciton to bound biexciton states. According to the level diagram (Figure 1a), the relative shift of the negative signal relative to the diagonal in emission energy is induced by the binding energy Δ_{XX} for attractive

biexciton interaction. The signal (II) is also elongated but not parallel to the diagonal, indicating that the value of Δ_{XX} varies with excitation energy. The excitation energy dependence of Δ_{XX} is an indication of the inhomogeneity effect on biexciton interactions.

There is an additional negative feature appearing with the emission energy above the probe energy ($\omega_t > \omega_\tau$). In principle, such a signal may be caused by the transition from $|X\rangle$ to "hot" biexciton state with a repulsive biexciton interaction. Nevertheless, the negative feature is partially dependent on polarization, suggesting that the transition to higher singly excited states likely makes the major contribution.[47,48] As proposed in the literature,[48] the transition is plausibly caused by the light-induced symmetry-breaking polaron in confined nanocrystals. The transition energy is predicted to increase with a decrease in nanocrystal size, which is consistent with the excitation energy dependence of such a negative feature.[48]

For better analysis of the inhomogeneity of Δ_{XX}, we plot the slice spectra recorded at different excitation energies (Figure 2a). The signals for the $|G\rangle \rightarrow |X\rangle$ transition are observed with resonant peaks at $\omega_\tau = \omega_t$. The line width of the exciton peak is ~1 meV as limited by the spectral resolution. The side peaks close to the resonant excitonic transitions are probably related to exciton–phonon coupling as discussed in detail in the Supporting Information.[49] The biexciton binding energy can thus be simply calculated as the difference in energy between the $|G\rangle \rightarrow |X\rangle$ and $|X\rangle \rightarrow |XX\rangle$ transitions as marked in Figure 2a. The value of Δ_{XX} increases from 25 to 40 meV when the excitation energy increases from 2340 to 2380 meV (Figure 2b).

Excitonic dynamics in perovskite semiconductor nanocrystals are highly sensitive to temperature. Figure 3 shows the data of 2DES measurements on the $CsPbBr_3$ nanocrystal film at different temperatures. With an increase in temperature, the resonant energy for the $|G\rangle \rightarrow |X\rangle$ transition gradually increases and the line width of the excitonic transition becomes broader (Figure 3a–c). To isolate the temperature effect, we take the value of E_X resonant to the absorption peak (Figure S2) at different temperatures (Figure 3d) that can be considered as the transition energy for a nanocrystal size of 9 nm. The temperature dependence of the exciton transition energy may be affected by thermal expansion, as well as the coupling of exciton to acoustic and multiple optical
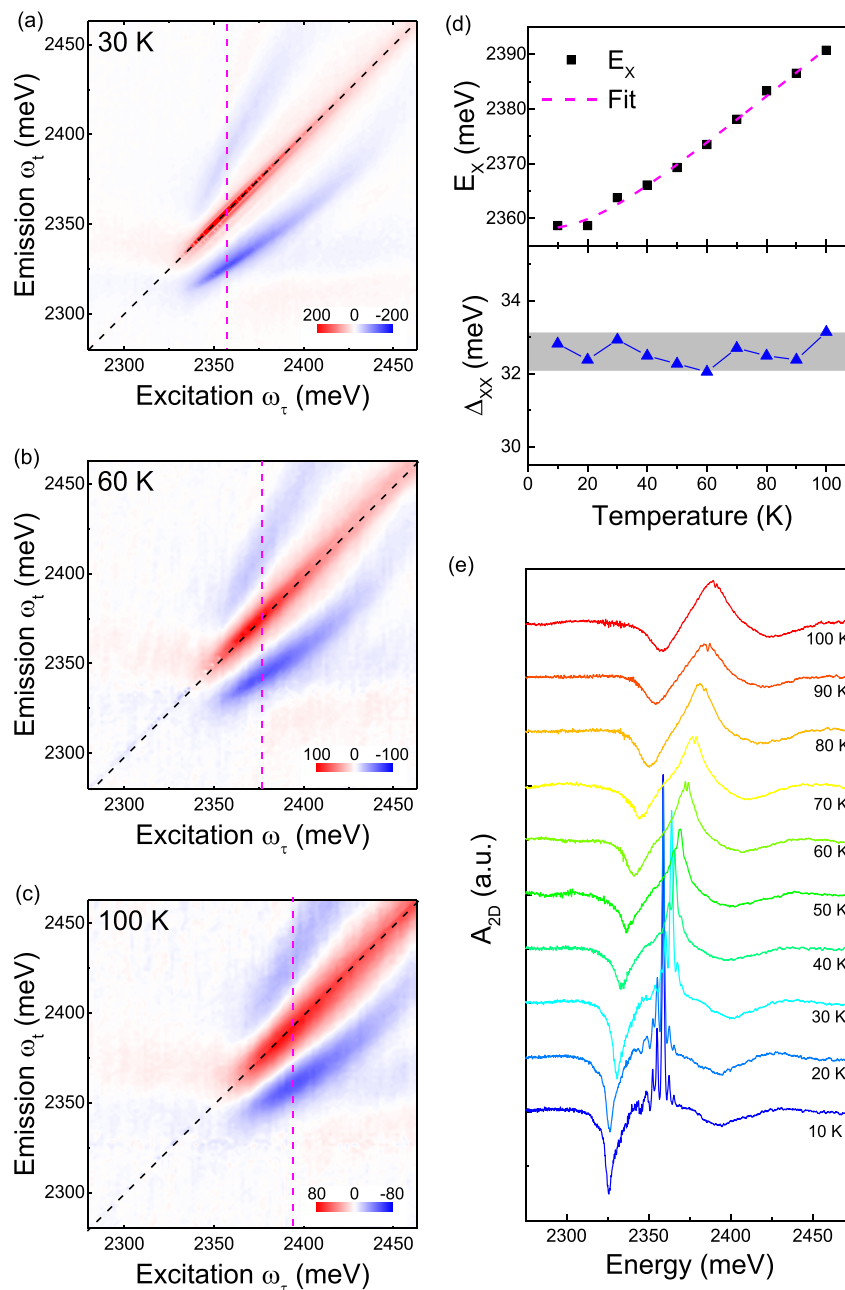
Figure 3. Temperature dependence of biexciton binding energy. Cross-circularly polarized 2D spectra measured at (a) 30, (b) 60, and (c) 90 K. The vertical lines represent the photon energies of the absorption peaks at different temperatures (Figure S2). (d) Temperature-dependent photon energy E_X resonant to absorption peak (top) and corresponding biexciton binding energy (bottom). (e) Sliced emission spectra recorded with excitation energies at the absorption peaks at different temperatures. The population delay time is 100 fs.

phonons.[42,50,51] For a phenomenological description, we consider two phonon modes to model the temperature (T_s)-dependent transition energy as[50,51]

$$E_X(T_s) = E_X(0) + A_1\left(\frac{1}{e^{E_1/k_B T_s} - 1} + \frac{1}{2}\right) + A_2\left(\frac{1}{e^{E_2/k_B T_s} - 1} + \frac{1}{2}\right) \quad (1)$$

where A_1 and A_2 are the electron−phonon coupling strengths for the two phonon modes with energies of E_1 and E_2, respectively. The experimental data can be reproduced with the following parameters: $E_X(0) = 2357$ meV, $A_1 = 17.4$ meV,

$E_1 = 3.4$ meV, $A_2 = -18$ meV, and $E_2 = 17$ meV. The two modes can roughly be considered as the acoustic and longitudinal optical modes,[52−54] respectively. Nevertheless, the value of Δ_{XX} is nearly unchanged (within a spectral resolution of ∼1 meV) when the temperature increases from 10 to 100 K (Figure 3d), suggesting that the biexciton binding strength is not sensitive to electron−phonon coupling.

The dephasing process of excitons is strongly dependent on temperature manifested as line width broadening in the spectral profile. The sliced spectra at different temperatures are shown in Figure 3e. With an increase in temperature, the spectral line width (Γ_X) for the $|G\rangle \rightarrow |X\rangle$ transition becomes broader due to exciton−phonon interaction,[55,56] where the fine structures become indistinguishable above 50 K. The line
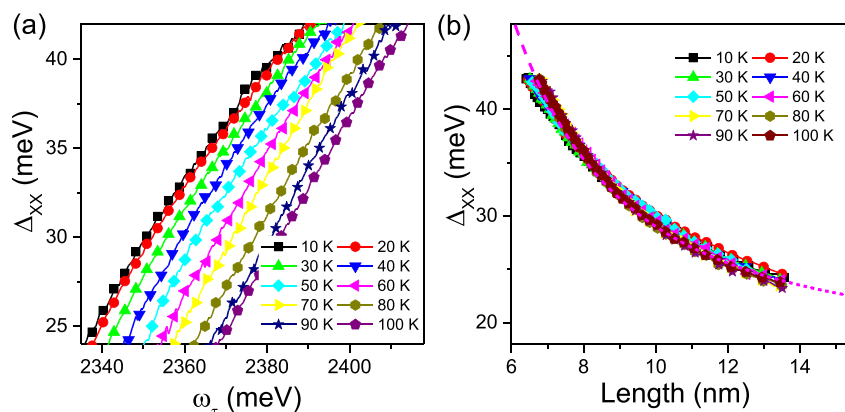
Figure 4. Size dependence of biexciton binding energy. (a) Excitation energy-dependent biexciton binding energy extracted from cross-circularly polarized 2D spectra at different temperatures. (b) Rescaled plot of Δ_{XX} (panel a) as a function of nanocrystal size using the EMA (eq 2). The dashed line shows a curve fitted to the function $\Delta_{XX} = C/r^2 + \Delta_0$.

width (Γ_{XX}) for the spectral feature of the $|X\rangle \rightarrow |XX\rangle$ transition is much less sensitive to the temperature. Remarkably, the line width for the $|X\rangle \rightarrow |XX\rangle$ transition is more than 8 times broader than that for the $|G\rangle \rightarrow |X\rangle$ excitonic transition at low temperatures. During single-dot spectroscopy of perovskite nanocrystals, the spectral line width for biexciton emission ($|XX\rangle \rightarrow |X\rangle$) is comparable to that of excitonic emission. According to the literature, such a discrepancy in the features of 2DES can be explained as a result of uncorrelated broadening between the $|G\rangle \rightarrow |X\rangle$ and $|X\rangle \rightarrow |XX\rangle$ transitions like the dynamics in the weakly confined GaAs quantum dots.[41] In other words, there are multiple biexciton transitions for a specific excitonic transition energy, which are probably caused by the multiple orbital configurations of excitonic dipoles,[49] the diverse shapes of perovskite nanocrystals,[57] and/or the effect of photocharging.[49,58] The uncorrelated broadening effect implies that it is insufficient to evaluate the biexciton energy with single-dot spectroscopic measurements on a limited number of nanocrystals, which should be carefully considered in demonstrating devices relying on coherent exciton–biexciton coupling.

Next, we analyze the size dependence of Δ_{XX} at different temperatures. Figure 4a shows the values of Δ_{XX} versus the excitation energy at different temperatures. In the concerned range, optical excitation is mainly induced by low-lying exciton transition. To quantify the size dependence, we establish the correlation between the transition energy and the nanocrystal size based on the EMA.[7,57,59] The size dependence of the excitonic transition at different temperatures (T) can be described as

$$E_X(T, r) = E_{BG}(T) - \Delta_X + \frac{\hbar^2 \pi^2}{2mr^2} \quad (2)$$

where $E_{BG}(T)$ is the temperature-dependent bulk value of the band gap and Δ_X is the bulk value of the exciton binding energy. The third term, $\Delta E_X(r) = \frac{\hbar^2 \pi^2}{2mr^2}$, is the size-dependent confinement energy assuming a spherical potential well with radius r for an exciton with an effective mass of m^*. The inverse quadratic size dependence of excitonic transition energy can reproduce the experimental data of cubically shaped CsPbBr$_3$ nanocrystals assuming edge length $a \sim r$ (Supporting Information).[7,57,59] In the temperature range concerned here (<100 K), the perovskite semiconductor

CsPbBr$_3$ is characterized with an orthorhombic structure. The reduced mass (m^*) equals $0.126m_0$ with a free electron mass of m_0.[60] The value of the exciton binding energy in CsPbBr$_3$ bulk material is 33 meV.[60] Temperature-dependent bulk band gap $E_{BG}(T)$ can be obtained with the experimental data for nanocrystals having $a = 9$ nm (Figure 3d). By neglecting the temperature dependences of m^* and Δ_X, we rescale the excitation energy-dependent Δ_{XX} (Figure 4a) as a function of nanocrystal size (Figure 4b). The value of biexciton binding energy can be reproduced as $\Delta_{XX} = C/r^2 + \Delta_0$ ($C = 1140$ meV nm^2; $\Delta_0 = 17.8$ meV), which is largely independent of temperature (Figure 4b).

The size-dependent biexciton binding energy in semiconductor quantum dots has been modeled by considering quantum and dielectric confinements with a variety of approaches.[19,61−66] The biexciton binding energy measured here can be explained well with the theoretical consideration in the weakly confined regime. The size dependence is mainly caused by the enhanced Coulomb interaction arising from the increased spatial overlap of excitons with a decreased nanocrystal size. For the size range studied in this work, the ratio between the confinement-induced modifications of biexciton energy and exciton energy $\eta = \Delta E_{XX}/\Delta E_X = 2m \times C/(\hbar^2 \pi^2)$ is ~0.38. That is, the size-dependent quantum confinement effect on the exciton binding energy in nanocrystals is ~2.6 times that for biexciton binding energy due to the greater attractive Coulomb force between electron–hole pairs than the Coulomb correlation between the exciton and exciton to form biexcitons. The ratio in CsPbBr$_3$ nanocrystals is much higher than that in conventional semiconductors of GaAs and ZnO,[67,68] implying that the biexcitons are less sensitive to quantum confinement than excitons in CsPbBr$_3$ nanocrystals. These differences are possibly related to the electronic structures of perovskite semiconductors with comparable effective masses of electrons and holes.

Next, we discuss the dynamics of the 2DES data. The decay of feature I can be described with two decay components with lifetime parameters of ~0.8 and ~20 ps (see Figure S5). As recently uncovered in CsPbI$_3$ nanocrystals,[69] the faster and slower components can be ascribed to spin depolarization caused by the excitonic response induced by Coulomb-mediated exchange interaction and free charge response induced by carrier–phonon interaction, respectively. The faster component dominates the decay dynamics of feature

II, which is consistent with the nature of the transition between bound excitonic states (i.e., from exciton to biexciton states). In previous TA spectroscopy studies, the biexciton feature exhibits a time-dependent "asymmetric" spectral characteristic that is induced by the "hot" biexciton effect.[32,46] Taking into account the capability of the excitation energy resolution of 2DES, our measurements mainly focus on the biexciton with excitation nearly resonant to the excitonic transitions in this work. The value of Δ_{XX} in the concerned range is nearly independent of the population delay time (Figure S5), which is reasonable because the hot carrier effect is largely excluded.

We now try to reconcile the diversely distributed results reported in the literature. Our measurements were conducted at cryogenic temperatures, while most literature results were obtained at room temperature. The temperature effect may cause some differences between the absolute values of biexciton binding energy. The value of Δ_{XX} evaluated in this work is comparable to the value measured by PL measurements at cryogenic temperatures.[70] 2DES allows quantification of the size-dependent biexciton binding strength with excitation fluence at a markedly low level. The merit is important for accessing the intrinsic value of the biexciton binding energy. The distributed values of Δ_{XX} reported in literatures can now be explained as a consequence of the size-dependent inhomogeneity in the nanocrystals with size diversity.[9,14,17,28−31] In comparison with the conventional methods of time-resolved spectroscopic measurements on ensemble samples, the significant size dependence may result in an overestimation of Δ_{XX} because the excitations may transfer from smaller nanocrystals to larger nanocrystals in the film samples. Another key issue is the high-fluence excitation required to generate the biexcitons in traditional techniques. Experimental results support the idea that high-fluence excitation creates some large particles in the samples exposed to air with bulklike emission.[30] Such an emission red-shift was perhaps considered as biexciton binding in previous measurements.[17] As the biexciton interaction is essential for gain generation in the semiconductor nanocrystals, the inhomogeneous biexciton binding and other extrinsic factors should be carefully considered in future demonstrations of perovskite nanocrystal devices. The charging effect is frequently observed in the perovskite nanocrystals, which is also manifested in the PL spectra (Figure S4). The response of charge excitons is not sensitive to pump polarization, which is not resolved in the 2DES spectra. Nevertheless, the involvement of the charge exciton may be a factor leading to the uncorrelated broadening of exciton- and biexciton-related transitions, which deserves more in-depth study in the future.

In summary, we have performed a 2DES study on biexciton binding in $CsPbBr_3$ nanocrystals at different temperatures. The biexciton binding energy, insensitive to the exciton−phonon interaction, increases nearly linearly with an increase in excitation energy showing an inverse-square size dependence under the EMA. The size-dependent biexciton binding in $CsPbBr_3$ nanocrystals can be understood with the model in the weakly confined regime where the Coulomb interaction is enhanced in small particles with increased spatial overlap of carrier wavefunction. In these weakly confined nanocrystals, the line width broadenings for the $|G\rangle \rightarrow |X\rangle$ and $|X\rangle \rightarrow |XX\rangle$ transitions are not fully correlated. The elucidation of the homogenous biexciton binding and uncorrelated broadening between the exciton and biexciton transitions is instrumental for demonstrating nanocrystal devices based on coherent exciton−biexciton interaction.

ASSOCIATED CONTENT

Supporting Information

The Supporting Information is available free of charge at https://pubs.acs.org/doi/10.1021/acs.jpclett.0c03153.

Sample preparation experimental details, transmission electron microscopy data of nanocrystals, temperature-dependent absorption spectra, power-dependent PL emission spectra, and population delay time-dependent 2DES data (PDF)

AUTHOR INFORMATION

Corresponding Authors

Chunfeng Zhang − National Laboratory of Solid State Microstructures, School of Physics, and Collaborative Innovation Center for Advanced Microstructures, Nanjing University, Nanjing 210093, China; ⓘ orcid.org/0000-0001-9030-5606; Email: cfzhang@nju.edu.cn

Min Xiao − National Laboratory of Solid State Microstructures, School of Physics, and Collaborative Innovation Center for Advanced Microstructures, Nanjing University, Nanjing 210093, China; Department of Physics, University of Arkansas, Fayetteville, Arkansas 72701, United States; Email: mxiao@nju.edu.cn

Authors

Xinyu Huang − National Laboratory of Solid State Microstructures, School of Physics, and Collaborative Innovation Center for Advanced Microstructures, Nanjing University, Nanjing 210093, China; ⓘ orcid.org/0000-0001-9962-4232

Lan Chen − National Laboratory of Solid State Microstructures, School of Physics, and Collaborative Innovation Center for Advanced Microstructures, Nanjing University, Nanjing 210093, China

Zhengyuan Qin − National Laboratory of Solid State Microstructures, School of Physics, and Collaborative Innovation Center for Advanced Microstructures, Nanjing University, Nanjing 210093, China

Buyang Yu − National Laboratory of Solid State Microstructures, School of Physics, and Collaborative Innovation Center for Advanced Microstructures, Nanjing University, Nanjing 210093, China

Xiaoyong Wang − National Laboratory of Solid State Microstructures, School of Physics, and Collaborative Innovation Center for Advanced Microstructures, Nanjing University, Nanjing 210093, China; ⓘ orcid.org/0000-0003-1147-0051

Complete contact information is available at:
https://pubs.acs.org/10.1021/acs.jpclett.0c03153

Author Contributions

§X.H. and L.C. contributed equally to this work.

Notes

The authors declare no competing financial interest.

■ REFERENCES

(1) Miyata, A.; Mitioglu, A.; Plochocka, P.; Portugall, O.; Wang, J. T.-W.; Stranks, S. D.; Snaith, H. J.; Nicholas, R. J. Direct measurement of the exciton binding energy and effective masses for charge carriers in organic-inorganic tri-halide perovskites. *Nat. Phys.* **2015**, *11* (7), 582.

(2) Sheng, C.; Zhang, C.; Zhai, Y.; Mielczarek, K.; Wang, W.; Ma, W.; Zakhidov, A.; Vardeny, Z. V. Exciton versus free carrier photogeneration in organometal trihalide perovskites probed by broadband ultrafast polarization memory dynamics. *Phys. Rev. Lett.* **2015**, *114* (11), 116601.

(3) D'Innocenzo, V.; Grancini, G.; Alcocer, M. J. P.; Kandada, A. R. S.; Stranks, S. D.; Lee, M. M.; Lanzani, G.; Snaith, H. J.; Petrozza, A. Excitons versus free charges in organo-lead tri-halide perovskites. *Nat. Commun.* **2014**, *5*, 3586.

(4) Saba, M.; Cadelano, M.; Marongiu, D.; Chen, F.; Sarritzu, V.; Sestu, N.; Figus, C.; Aresti, M.; Piras, R.; Geddo Lehmann, A.; Cannas, C.; Musinu, A.; Quochi, F.; Mura, A.; Bongiovanni, G. Correlated electron-hole plasma in organometal perovskites. *Nat. Commun.* **2014**, *5*, 5049.

(5) Akkerman, Q. A.; Rainò, G.; Kovalenko, M. V.; Manna, L. Genesis, challenges and opportunities for colloidal lead halide perovskite nanocrystals. *Nat. Mater.* **2018**, *17* (5), 394.

(6) Kovalenko, M. V.; Protesescu, L.; Bodnarchuk, M. I. Properties and potential optoelectronic applications of lead halide nanocrystals. *Science* **2017**, *358* (6364), 745–750.

(7) Protesescu, L.; Yakunin, S.; Bodnarchuk, M. I.; Krieg, F.; Caputo, R.; Hendon, C. H.; Yang, R. X.; Walsh, A.; Kovalenko, M. V. Nanocrystals of cesium lead halide perovskites (cspbx₃, x = cl, br, and i): Novel optoelectronic materials showing bright emission with wide color gamut. *Nano Lett.* **2015**, *15* (6), 3692–3696.

(8) Yakunin, S.; Protesescu, L.; Krieg, F.; Bodnarchuk, M. I.; Nedelcu, G.; Humer, M.; De Luca, G.; Fiebig, M.; Heiss, W.; Kovalenko, M. V. Low-threshold amplified spontaneous emission and lasing from colloidal nanocrystals of caesium lead halide perovskites. *Nat. Commun.* **2015**, *6*, 8056.

(9) Wang, Y.; Li, X.; Song, J.; Xiao, L.; Zeng, H.; Sun, H. All-inorganic colloidal perovskite quantum dots: A new class of lasing materials with favorable characteristics. *Adv. Mater.* **2015**, *27* (44), 7101.

(10) Zhang, X.; Sun, C.; Zhang, Y.; Wu, H.; Ji, C.; Chuai, Y.; Wang, P.; Wen, S.; Zhang, C.; Yu, W. W. Bright perovskite nanocrystal films for efficient light-emitting devices. *J. Phys. Chem. Lett.* **2016**, *7* (22), 4602–4610.

(11) Takemura, N.; Trebaol, S.; Wouters, M.; Portella-Oberli, M. T.; Deveaud, B. Polaritonic feshbach resonance. *Nat. Phys.* **2014**, *10* (7), 500–504.

(12) Su, R.; Diederichs, C.; Wang, J.; Liew, T. C. H.; Zhao, J.; Liu, S.; Xu, W.; Chen, Z.; Xiong, Q. Room-temperature polariton lasing in all-inorganic perovskite nanoplatelets. *Nano Lett.* **2017**, *17* (6), 3982–3988.

(13) Hu, F.; Zhang, H.; Sun, C.; Yin, C.; Lv, B.; Zhang, C.; Yu, W. W.; Wang, X.; Zhang, Y.; Xiao, M. Superior optical properties of perovskite nanocrystals as single photon emitters. *ACS Nano* **2015**, *9* (12), 12410–12416.

(14) Makarov, N. S.; Guo, S. J.; Isaienko, O.; Liu, W. Y.; Robel, I.; Klimov, V. I. Spectral and dynamical properties of single excitons, biexcitons, and trions in cesium-lead-halide perovskite quantum dots. *Nano Lett.* **2016**, *16* (4), 2349–2362.

(15) Lv, Y.; Yin, C.; Zhang, C.; Yu, W. W.; Wang, X.; Zhang, Y.; Xiao, M. Quantum interference in a single perovskite nanocrystal. *Nano Lett.* **2019**, *19* (7), 4442–4447.

(16) Utzat, H.; Sun, W.; Kaplan, A. E. K.; Krieg, F.; Ginterseder, M.; Spokoyny, B.; Klein, N. D.; Shulenberger, K. E.; Perkinson, C. F.; Kovalenko, M. V.; Bawendi, M. G. Coherent single-photon emission from colloidal lead halide perovskite quantum dots. *Science* **2019**, *363* (6431), 1068.

(17) Castañeda, J. A.; Nagamine, G.; Yassitepe, E.; Bonato, L. G.; Voznyy, O.; Hoogland, S.; Nogueira, A. F.; Sargent, E. H.; Cruz, C. H. B.; Padilha, L. A. Efficient biexciton interaction in perovskite quantum dots under weak and strong confinement. *ACS Nano* **2016**, *10* (9), 8603–8609.

(18) Chen, J.; Zhang, Q.; Shi, J.; Zhang, S.; Du, W.; Mi, Y.; Shang, Q.; Liu, P.; Sui, X.; Wu, X.; Wang, R.; Peng, B.; Zhong, H.; Xing, G.; Qiu, X.; Sum, T. C.; Liu, X. Room temperature continuous-wave excited biexciton emission in perovskite nanoplatelets via plasmonic nonlinear fano resonance. *Commun. Phys.* **2019**, *2*, 80.

(19) Nguyen, T. P. T.; Blundell, S. A.; Guet, C. Calculation of the biexciton shift in nanocrystals of inorganic perovskites. *Phys. Rev. B: Condens. Matter Mater. Phys.* **2020**, *101* (12), 125424.

(20) Li, M.; Begum, R.; Fu, J.; Xu, Q.; Koh, T. M.; Veldhuis, S. A.; Graetzel, M.; Mathews, N.; Mhaisalkar, S.; Sum, T. C. Low threshold and efficient multiple exciton generation in halide perovskite nanocrystals. *Nat. Commun.* **2018**, *9*, 4197.

(21) Zhao, W.; Qin, Z.; Zhang, C.; Wang, G.; Huang, X.; Li, B.; Dai, X.; Xiao, M. Optical gain from biexcitons in cspbbr3 nanocrystals revealed by two-dimensional electronic spectroscopy. *J. Phys. Chem. Lett.* **2019**, *10* (6), 1251–1258.

(22) Xu, Y.; Chen, Q.; Zhang, C.; Wang, R.; Wu, H.; Zhang, X.; Xing, G.; Yu, W. W.; Wang, X.; Zhang, Y.; Xiao, M. Two-photon-pumped perovskite semiconductor nanocrystal lasers. *J. Am. Chem. Soc.* **2016**, *138* (11), 3761–3768.

(23) Bennett, A. J.; Pooley, M. A.; Stevenson, R. M.; Ward, M. B.; Patel, R. B.; de la Giroday, A. B.; Skoeld, N.; Farrer, I.; Nicoll, C. A.; Ritchie, D. A.; Shields, A. J. Electric-field-induced coherent coupling of the exciton states in a single quantum dot. *Nat. Phys.* **2010**, *6* (12), 947–950.

(24) Stevenson, R. M.; Salter, C. L.; Nilsson, J.; Bennett, A. J.; Ward, M. B.; Farrer, I.; Ritchie, D. A.; Shields, A. J. Indistinguishable entangled photons generated by a light-emitting diode. *Phys. Rev. Lett.* **2012**, *108* (4), 040503.

(25) Stevenson, R. M.; Young, R. J.; Atkinson, P.; Cooper, K.; Ritchie, D. A.; Shields, A. J. A semiconductor source of triggered entangled photon pairs. *Nature* **2006**, *439* (7073), 179–182.

(26) Suzuki, T.; Singh, R.; Bayer, M.; Ludwig, A.; Wieck, A. D.; Cundiff, S. T. Coherent control of the exciton-biexciton system in an inas self-assembled quantum dot ensemble. *Phys. Rev. Lett.* **2016**, *117* (15), 157402.

(27) Klingshirn, C. F. *Semiconductor optics*; Springer Science & Business Media, 2012.

(28) Ashner, M. N.; Shulenberger, K. E.; Krieg, F.; Powers, E. R.; Kovalenko, M. V.; Bawendi, M. G.; Tisdale, W. A. Size-dependent biexciton spectrum in cspbbr3 perovskite nanocrystals. *ACS Energy Lett.* **2019**, *4* (11), 2639–2645.

(29) Mondal, A.; Aneesh, J.; Kumar Ravi, V.; Sharma, R.; Mir, W. J.; Beard, M. C.; Nag, A.; Adarsh, K. V. Ultrafast exciton many-body interactions and hot-phonon bottleneck in colloidal cesium lead halide perovskite nanocrystals. *Phys. Rev. B: Condens. Matter Mater. Phys.* **2018**, *98* (11), 115418.

(30) Shulenberger, K. E.; Ashner, M. N.; Ha, S. K.; Krieg, F.; Kovalenko, M. V.; Tisdale, W. A.; Bawendi, M. G. Setting an upper bound to the biexciton binding energy in cspbbr3 perovskite nanocrystals. *J. Phys. Chem. Lett.* **2019**, *10*, 5680–5686.

(31) Aneesh, J.; Swarnkar, A.; Kumar Ravi, V.; Sharma, R.; Nag, A.; Adarsh, K. V. Ultrafast exciton dynamics in colloidal cspbbr3 perovskite nanocrystals: Biexciton effect and auger recombination. *J. Phys. Chem. C* **2017**, *121* (8), 4734–4739.

(32) Yumoto, G.; Tahara, H.; Kawawaki, T.; Saruyama, M.; Sato, R.; Teranishi, T.; Kanemitsu, Y. Hot biexciton effect on optical gain in cspbi3 perovskite nanocrystals. *J. Phys. Chem. Lett.* **2018**, *9* (9), 2222−2228.

(33) Jonas, D. M. Two-dimensional femtosecond spectroscopy. *Annu. Rev. Phys. Chem.* **2003**, *54* (1), 425−463.

(34) Camargo, F. V. A.; Nagahara, T.; Feldmann, S.; Richter, J. M.; Friend, R. H.; Cerullo, G.; Deschler, F. Dark subgap states in metal-halide perovskites revealed by coherent multidimensional spectroscopy. *J. Am. Chem. Soc.* **2020**, *142* (2), 777−782.

(35) Seiler, H.; Palato, S.; Sonnichsen, C.; Baker, H.; Socie, E.; Strandell, D. P.; Kambhampati, P. Two-dimensional electronic spectroscopy reveals liquid-like lineshape dynamics in cspbi3 perovskite nanocrystals. *Nat. Commun.* **2019**, *10*, 4962.

(36) Gellen, T. A.; Lem, J.; Turner, D. B. Probing homogeneous line broadening in cdse nanocrystals using multidimensional electronic spectroscopy. *Nano Lett.* **2017**, *17* (5), 2809−2815.

(37) Elkins, M. H.; Pensack, R.; Proppe, A. H.; Voznyy, O.; Quan, L. N.; Kelley, S. O.; Sargent, E. H.; Scholes, G. D. Biexciton resonances reveal exciton localization in stacked perovskite quantum wells. *J. Phys. Chem. Lett.* **2017**, *8* (16), 3895−3901.

(38) Li, X. Q.; Zhang, T. H.; Borca, C. N.; Cundiff, S. T. Many-body interactions in semiconductors probed by optical two-dimensional fourier transform spectroscopy. *Phys. Rev. Lett.* **2006**, *96* (5), 057406.

(39) Stone, K. W.; Gundogdu, K.; Turner, D. B.; Li, X.; Cundiff, S. T.; Nelson, K. A. Two-quantum 2d ft electronic spectroscopy of biexcitons in gaas quantum wells. *Science* **2009**, *324* (5931), 1169−1173.

(40) Moody, G.; Singh, R.; Li, H.; Akimov, I.; Bayer, M.; Reuter, D.; Wieck, A.; Bracker, A.; Gammon, D.; Cundiff, S. Influence of confinement on biexciton binding in semiconductor quantum dot ensembles measured with two-dimensional spectroscopy. *Phys. Rev. B: Condens. Matter Mater. Phys.* **2013**, *87* (4), 041304.

(41) Moody, G.; Singh, R.; Li, H.; Akimov, I.; Bayer, M.; Reuter, D.; Wieck, A.; Cundiff, S. Fifth-order nonlinear optical response of excitonic states in an inas quantum dot ensemble measured with two-dimensional spectroscopy. *Phys. Rev. B: Condens. Matter Mater. Phys.* **2013**, *87* (4), 045313.

(42) Zhu, W.; Wang, R.; Zhang, C.; Wang, G.; Liu, Y.; Zhao, W.; Dai, X.; Wang, X.; Cerullo, G.; Cundiff, S.; Xiao, M. Broadband two-dimensional electronic spectroscopy in an actively phase stabilized pump-probe configuration. *Opt. Express* **2017**, *25* (18), 21115.

(43) Bristow, A. D.; Karaiskaj, D.; Dai, X.; Zhang, T.; Carlsson, C.; Hagen, K. R.; Jimenez, R.; Cundiff, S. T. A versatile ultrastable platform for optical multidimensional fourier-transform spectroscopy. *Rev. Sci. Instrum.* **2009**, *80* (7), 073108.

(44) Bristow, A. D.; Karaiskaj, D.; Dai, X.; Mirin, R. P.; Cundiff, S. T. Polarization dependence of semiconductor exciton and biexciton contributions to phase-resolved optical two-dimensional fourier-transform spectra. *Phys. Rev. B: Condens. Matter Mater. Phys.* **2009**, *79* (16), 161305.

(45) Steinhoff, A.; Florian, M.; Singh, A.; Tran, K.; Kolarczik, M.; Helmrich, S.; Achtstein, A. W.; Woggon, U.; Owschimikow, N.; Jahnke, F.; Li, X. Biexciton fine structure in monolayer transition metal dichalcogenides. *Nat. Phys.* **2018**, *14* (12), 1199.

(46) Kobiyama, E.; Tahara, H.; Sato, R.; Saruyama, M.; Teranishi, T.; Kanemitsu, Y. Reduction of optical gain threshold in cspbi3 nanocrystals achieved by generation of asymmetric hot-biexcitons. *Nano Lett.* **2020**, *20* (5), 3905−3910.

(47) Li, Y. L.; Luo, X.; Liu, Y.; Lu, X.; Wu, K. F. Size- and composition-dependent exciton spin relaxation in lead halide perovskite quantum dots. *ACS Energy Lett.* **2020**, *5* (5), 1701−1708.

(48) Rossi, D.; Wang, H.; Dong, Y.; Qiao, T.; Qian, X.; Son, D. H. Light-induced activation of forbidden exciton transition in strongly confined perovskite quantum dots. *ACS Nano* **2018**, *12* (12), 12436−12443.

(49) Fu, M.; Tamarat, P.; Huang, H.; Even, J.; Rogach, A. L.; Lounis, B. Neutral and charged exciton fine structure in single lead halide perovskite nanocrystals revealed by magneto-optical spectroscopy. *Nano Lett.* **2017**, *17* (5), 2895−2901.

(50) Saran, R.; Heuer-Jungemann, A.; Kanaras, A. G.; Curry, R. J. Giant bandgap renormalization and exciton−phonon scattering in perovskite nanocrystals. *Adv. Opt. Mater.* **2017**, *5* (17), 1700231.

(51) Bhosale, J.; Ramdas, A. K.; Burger, A.; Munoz, A.; Romero, A. H.; Cardona, M.; Lauck, R.; Kremer, R. K. Temperature dependence of band gaps in semiconductors: Electron-phonon interaction. *Phys. Rev. B: Condens. Matter Mater. Phys.* **2012**, *86* (19), 195208.

(52) Yang, J.; Wen, X.; Xia, H.; Sheng, R.; Ma, Q.; Kim, J.; Tapping, P.; Harada, T.; Kee, T. W.; Huang, F.; Cheng, Y.-B.; Green, M.; Ho-Baillie, A.; Huang, S.; Shrestha, S.; Patterson, R.; Conibeer, G. Acoustic-optical phonon up-conversion and hot-phonon bottleneck in lead-halide perovskites. *Nat. Commun.* **2017**, *8*, 14120.

(53) Granados del Aguila, A.; Do, T. T. H.; Xing, J.; Jee, W. J.; Khurgin, J. B.; Xiong, Q. Efficient up-conversion photoluminescence in all-inorganic lead halide perovskite nanocrystals. *Nano Res.* **2020**, *13*, 1962.

(54) Wright, A. D.; Verdi, C.; Milot, R. L.; Eperon, G. E.; Perez-Osorio, M. A.; Snaith, H. J.; Giustino, F.; Johnston, M. B.; Herz, L. M. Electron-phonon coupling in hybrid lead halide perovskites. *Nat. Commun.* **2016**, *7*, 11755.

(55) Fu, M.; Tamarat, P.; Trebbia, J.-B.; Bodnarchuk, M. I.; Kovalenko, M. V.; Even, J.; Lounis, B. Unraveling exciton-phonon coupling in individual fapbi(3) nanocrystals emitting near-infrared single photons. *Nat. Commun.* **2018**, *9*, 3318.

(56) Moody, G.; Kavir Dass, C.; Hao, K.; Chen, C.-H.; Li, L.-J.; Singh, A.; Tran, K.; Clark, G.; Xu, X.; Berghäuser, G.; Malic, E.; Knorr, A.; Li, X. Intrinsic homogeneous linewidth and broadening mechanisms of excitons in monolayer transition metal dichalcogenides. *Nat. Commun.* **2015**, *6* (1), 8315.

(57) Lin, J.; Gomez, L.; de Weerd, C.; Fujiwara, Y.; Gregorkiewicz, T.; Suenaga, K. Direct observation of band structure modifications in nanocrystals of cspbbr3 perovskite. *Nano Lett.* **2016**, *16* (11), 7198−7202.

(58) Yin, C.; Chen, L.; Song, N.; Lv, Y.; Hu, F.; Sun, C.; Yu, W. W.; Zhang, C.; Wang, X.; Zhang, Y.; Xiao, M. Bright-exciton fine-structure splittings in single perovskite nanocrystals. *Phys. Rev. Lett.* **2017**, *119* (2), 026401.

(59) Butkus, J.; Vashishtha, P.; Chen, K.; Gallaher, J. K.; Prasad, S. K. K.; Metin, D. Z.; Laufersky, G.; Gaston, N.; Halpert, J. E.; Hodgkiss, J. M. The evolution of quantum confinement in cspbbr3 perovskite nanocrystals. *Chem. Mater.* **2017**, *29* (8), 3644−3652.

(60) Yang, Z.; Surrente, A.; Galkowski, K.; Miyata, A.; Portugall, O.; Sutton, R. J.; Haghighirad, A. A.; Snaith, H. J.; Maude, D. K.; Plochocka, P.; Nicholas, R. J. Impact of the halide cage on the electronic properties of fully inorganic cesium lead halide perovskites. *ACS Energy Lett.* **2017**, *2* (7), 1621−1627.

(61) Langbein, W.; Hvam, J. M. Localization-enhanced biexciton binding in semiconductors. *Phys. Rev. B: Condens. Matter Mater. Phys.* **1999**, *59* (23), 15405−15408.

(62) Schliwa, A.; Winkelnkemper, M.; Bimberg, D. Few-particle energies versus geometry and composition of inxga1-xas/gaas self-organized quantum dots. *Phys. Rev. B: Condens. Matter Mater. Phys.* **2009**, *79* (7), 075443.

(63) Ikezawa, M.; Masumoto, Y.; Takagahara, T.; Nair, S. V. Biexciton and triexciton states in quantum dots in the weak confinement regime. *Phys. Rev. Lett.* **1997**, *79* (18), 3522−3525.

(64) Hu, Y. Z.; Lindberg, M.; Koch, S. W. Theory of optically-excited intrinsic semiconductor quantum dots. *Phys. Rev. B: Condens. Matter Mater. Phys.* **1990**, *42* (3), 1713−1723.

(65) Takagahara, T. Biexciton states in semiconductor quantum dots and their nonlinear optical-properties. *Phys. Rev. B: Condens. Matter Mater. Phys.* **1989**, *39* (14), 10206−10231.

(66) Usukura, J.; Suzuki, Y.; Varga, K. Stability of two- and three-dimensional excitonic complexes. *Phys. Rev. B: Condens. Matter Mater. Phys.* **1999**, *59* (8), 5652−5661.

(67) Birkedal, D.; Singh, J.; Lyssenko, V. G.; Erland, J.; Hvam, J. M. Binding of quasi-two-dimensional biexcitons. *Phys. Rev. Lett.* **1996**, *76* (4), 672−675.

(68) Hvam, J. M. Excitonic molecule transitions in zno. *Phys. Status Solidi B* **1979**, *93* (2), 581−590.

(69) Strohmair, S.; Dey, A.; Tong, Y.; Polavarapu, L.; Bohn, B. J.; Feldmann, J. Spin polarization dynamics of free charge carriers in cspbi3 nanocrystals. *Nano Lett.* **2020**, *20* (7), 4724−4730.

(70) Shinde, A.; Gahlaut, R.; Mahamuni, S. Low-temperature photoluminescence studies of cspbbr3 quantum dots. *J. Phys. Chem. C* **2017**, *121* (27), 14872−14878.